J. Fluid Mech. (1989), *vol.* 208, *pp.* 45–66
Printed in Great Britain

Numerical simulations of transition in oscillatory plane channel flow

By BART A. SINGER[1], JOEL H. FERZIGER[2] AND HELEN L. REED[3]

[1] High Technology Corp., 28 Research Drive, Hampton, VA 23666, USA
[2] Stanford University, Stanford, CA 94305, USA
[3] Arizona State University, Tempe, AZ 85287, USA

(Received 16 November 1988 and in revised form 17 March 1989)

The effect of flow oscillation on the stability of plane channel flow is studied via numerical simulation. For weak oscillation, the ratio of the Stokes layer thickness to the distance from the wall to the critical layer in steady flow provides the best normalization for the mean-flow frequency. Maximum growth rates occur when the instantaneous velocity profile has large regions of positive curvature. The effect of oscillation is generally stabilizing. However, at low frequencies, TS wave energies may vary by 10^6 in a cycle and irreversible secondary instability may be produced at the peak.

1. Introduction

Laminar–turbulent transition in the presence of an unsteady mean flow is a fundamental problem in fluid mechanics. While many types of mean unsteadiness are possible, in this paper we study the idealized problem of oscillatory flow in a plane channel in order to obtain insight as to how flow periodicity influences the transition process. Very little previous work has been done on this problem.

Grosch & Salwen (1968) integrated the linearized equations through one period of oscillation. The maximum growth rate was determined by solving the resultant eigenvalue problem. For small mean velocity perturbations the modulated flow was more stable than the steady flow. Larger fluctuations produced an abnormally strong instability. The validity of this result has been questioned by other researchers.

Herbert (1972) performed an energy analysis for small modulation amplitudes. He examined the energy transfer process in the thin shear layer at the wall and found that mean flow frequencies greater than $\frac{1}{4}$ the frequency of a disturbance wave make the flow more stable. He emphasized the importance of the interaction of the unsteady portion of the mean flow with the disturbance.

Hall (1975) studied the stability characteristics of oscillatory plane Poiseuille flow for high frequency modulations. He matched expansions for the very thin Stokes layer with those of the outer flow and concluded that high-frequency oscillations have a slightly destabilizing effect.

Von Kerczek (1982) performed a perturbation analysis of the linear equations about the critical Reynolds number. He found that modulation frequencies near that of the most unstable Tollmien–Schlichting (T–S) wave of the steady case stabilized the flow. At the critical Reynolds number of 5772.22 both very low and very high frequencies tend to make the flow mildly unstable. He did not find any strongly unstable modes, in conflict with the results of Grosch & Salwen (1968).

In this work, the problem is approached via direct numerical simulations of the full Navier–Stokes equations as well as two-dimensional linear simulations. We start by describing the time-dependent mean flow, paying special attention to factors that may be important during transition. We continue with a discussion of linear development. Finally, we connect these results with fully three-dimensional, nonlinear simulation results.

2. The mean flow

The flow considered is that between two parallel plates of infinite extent in the streamwise and spanwise directions. The streamwise direction is denoted by x or x_1, the direction normal to the walls by y or x_2, and the spanwise direction by z or x_3. All quantities are non-dimensionalized using the channel half-width, h, the centreline velocity of the steady laminar flow, U_0, and the density, ρ. The Reynolds number is $Re = U_0 h/\nu$ where ν is the kinematic viscosity. The domain extends from -1 to 1 in the normal direction with 0 on the centreline. The flow is driven by an unsteady pressure gradient,

$$\frac{\mathrm{d}p}{\mathrm{d}x} = -\frac{2}{Re}(1+N\cos(tS)), \tag{2.1}$$

where the relative amplitude of the pressure oscillation is N, the frequency of oscillation is Ω^*, the Strouhal number is $S = \Omega^* h/U_0$, and time is non-dimensionalized by h/U_0. The mean flow is given by

$$U(y) = 1-y^2+\Delta\sin(tS) - \frac{\Delta\left[\cos(tS)\,(b(y)\,a(1)-b(1)\,a(y))+\sin(tS)\,(a(y)\,a(1)+b(y)\,b(1))\right]}{a(1)^2+b(1)^2} \tag{2.2}$$

where

$$\left.\begin{aligned} a(y) &= \cos[(ReS/2)^{\frac{1}{2}}y]\cosh[(ReS/2)^{\frac{1}{2}}y],\\ b(y) &= \sin[(ReS/2)^{\frac{1}{2}}y]\sinh[(ReS/2)^{\frac{1}{2}}y],\end{aligned}\right\} \tag{2.3}$$

and $\Delta = 2N/SRe$ is the maximum fractional change in the mean flow velocity. The velocity consists of three parts. The first is the parabolic profile, $1-y^2$, representing the time-mean or steady laminar flow. The second term, $\Delta\sin(tS)$, represents the displacement of the bulk flow velocity with no change in shape; it is the effect the pressure oscillation would produce in the absence of walls. The remaining terms are needed to satisfy the no-slip boundary condition; they represent Stokes layers near the walls which become thinner as the Strouhal and/or Reynolds number increases. The presence of the Stokes layers is the most important effect of the unsteadiness. The non-dimensional thickness of the Stokes layer is $\delta = [2/ReS)]^{\frac{1}{2}}$. In the parameter range studied here, $0.01 < \delta < 0.2$.

Figure 1 (*a–d*) shows the mean velocity profiles at four different phases for $Re = 5000$, $S = 0.1052$, and $\Delta = 0.10$. For this flow, $\delta = 0.06$. Of particular importance are inflection points in the profile. Figure 1 (*a*) shows the velocity profile at $t = 14.93$, just before inflection points develop at each wall. At 29.87 (figure 1*b*) there are inflection points at $y = \pm 0.92$. The inflection points slowly migrate toward the channel centre. When they reach $y = \pm 0.85$, new inflection points develop at each wall and all four inflection points move toward the channel centre. The profile at $t = 44.81$ (figure 1*c*) contains two inflection points near each wall; the extent of the region of positive curvature is $\Delta y \approx 0.15$ and is approximately the largest extent of positive curvature. As time progresses, the inflection points nearer the channel centre

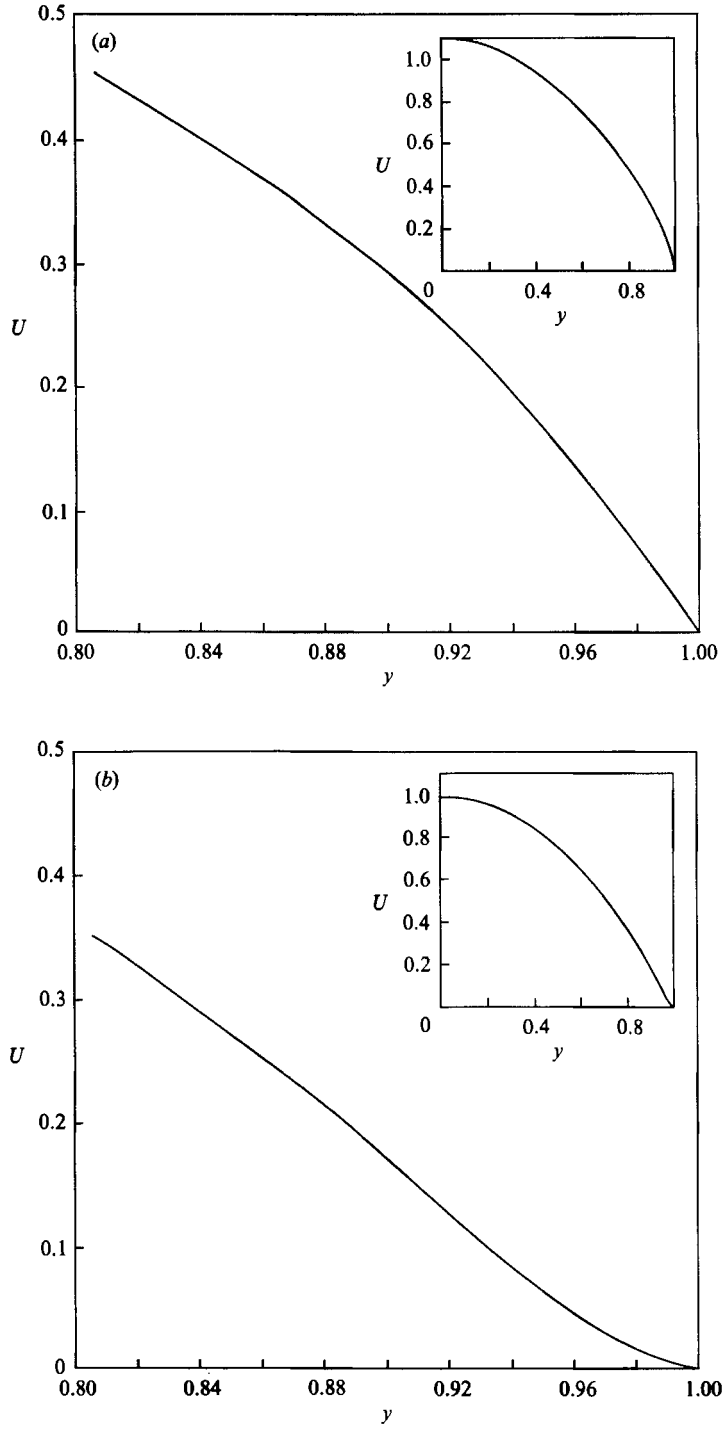

FIGURE 1 (*a*, *b*). For caption see next page.

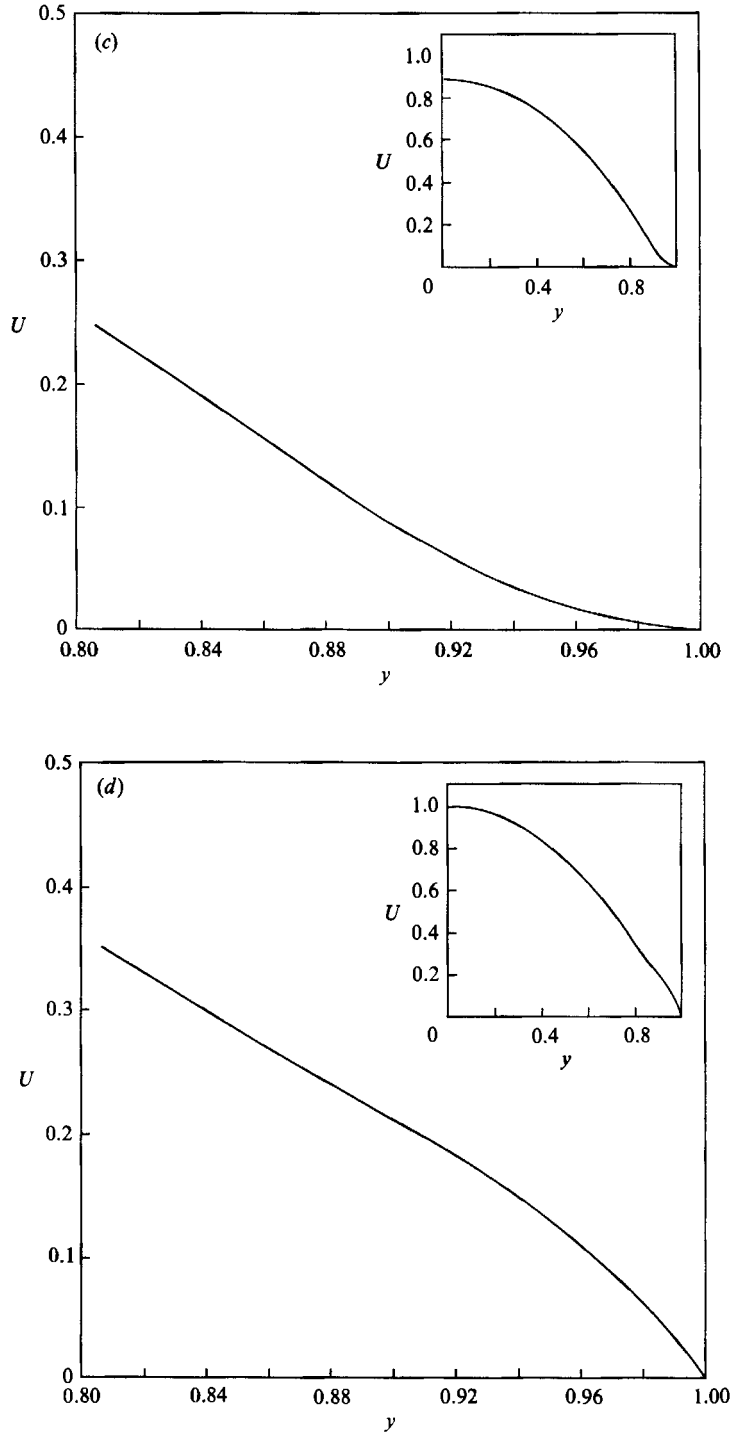

FIGURE 1. Mean flow near upper wall (channel upper half in insert) at various times and $Re = 5000$, $S = 0.1051667$, $\Delta = 0.10$. (*a*) $t = 14.93$, (*b*) 29.87, (*c*) 44.81, (*d*) 59.74.

change their direction of motion and move towards the wall. The profile at $t = 59.74$ contains inflection points at $y = \pm 0.89$ and $y = \pm 0.80$. These two inflection points continue to approach each other and finally coalesce and disappear at $t = 64.9$.

3. Linear theory

3.1. *Analysis*

The available results of linear stability theory for oscillating plane Poiseuille flow are in serious disagreement. Grosch & Salwen (1968) found highly unstable modes for large-amplitude pressure gradient modulation while von Kerczek (1982) indicated that such modes do not exist. To obtain reliable results against which full simulation results can be checked, we recomputed the linear behaviour. This will also help clear up the discrepancy.

To determine the most unstable modes for flow in a plane channel subject to a sinusoidally varying pressure gradient, we employ a linear theory similar to that of Grosch & Salwen (1968). This involves integrating the linearized Navier–Stokes equations for a full period of the oscillation. The pressure and stream function are assumed to have the form

$$\left.\begin{aligned} p(x,y,t) &= -\frac{2}{Re}x(1+N\sin(tS))+\hat{p}(y,t)\exp(\mathrm{i}k_x x),\\ \psi(x,y,t) &= \phi(y,t)\exp(\mathrm{i}k_x x). \end{aligned}\right\} \tag{3.1}$$

Substituting these into the Navier–Stokes equations, linearizing and eliminating the pressure we find an equation for ϕ:

$$\frac{\partial[\phi''-k_x^2\phi]}{\partial t} = \frac{1}{Re}[\phi''''-2k_x^2\phi''+k_x^4\phi]+\mathrm{i}k_x[U''\phi-U\phi''+k_x^2U\phi], \tag{3.2}$$

where a prime indicates differentiation with respect to y. The no-slip and impermeability boundary conditions become

$$\phi = \phi' = 0 \quad \text{at} \quad y = \pm 1. \tag{3.3}$$

To solve this equation, we expand ϕ in a generalized Fourier series

$$\phi = \sum_n g_n(t)\,\phi_n(y), \tag{3.4}$$

where each expansion function satisfies the boundary conditions. The work of Moser, Moin & Leonard (1983) suggests a convenient choice:

$$\phi_n(y) = (1-y^2)^2 P_n(y), \tag{3.5}$$

where $P_n(y)$ is the Legendre polynomial of order n. Legendre polynomials provide good resolution near the wall (Gottlieb & Orszag 1981) where the effects of the pressure modulation are most important. Multiplying (3.2) by ϕ_m and integrating across the channel gives

$$\boldsymbol{A}\frac{\mathrm{d}\boldsymbol{g}}{\mathrm{d}t} = \boldsymbol{B}\boldsymbol{g}+\boldsymbol{C}\boldsymbol{g}. \tag{3.6}$$

The vector $\boldsymbol{g}$ is composed of the unknown coefficients $g_n(t)$. The matrices $\boldsymbol{A}$ and $\boldsymbol{B}$ are

time-independent banded symmetric matrices. Integration by parts allows us to write their elements as

$$A_{m,n} = -\int_{-1}^{1} (k_x^2 \phi_m \phi_n + \phi'_m \phi'_n) \mathrm{d}y \tag{3.7}$$

and

$$B_{m,n} = \frac{1}{Re} \int_{-1}^{1} (\phi''_m \phi''_n + 2k_x^2 \phi'_m \phi'_n + k_x^4 \phi_m \phi_n) \, \mathrm{d}y. \tag{3.8}$$

The integrals in (3.7) and (3.8) can be evaluated using the orthogonality properties of Legendre polynomials. The matrix $\boldsymbol{C}$ contains the convective terms and must be recomputed at each time step using the unsteady mean velocity profile U. Its elements are

$$C_{m,n} = \mathrm{i}k_x \int_{-1}^{1} [(U'' + k_x^2) \phi_m \phi_n + U \phi'_m \phi'_n + U' \phi_m \phi'_n] \, \mathrm{d}y. \tag{3.9}$$

Lobatto quadrature (similar to Gauss quadrature but with the coordinates of the endpoints fixed, see Abramowitz & Stegun 1972) is used to compute the right-hand side of (3.9). If N grid points (including ± 1) are used, the y-location of the ith grid point is the $(i-1)$th zero of P'_{N-1}. Lobatto quadrature exactly integrates any polynomial of degree less than or equal to $2N-3$, hence the integrand in (3.9) must satisfy this constraint. The values of the velocity U are required at the N collocation points; this is equivalent to replacing U by an $(N-1)$-order polynomial through the points. To obtain an exact result, the maximum order, M, of the polynomial in the expansion functions, ϕ, must satisfy $2M+N-3 \leqslant 2N-3$ or $M \leqslant \frac{1}{2}N$. This relation is similar to the $\frac{2}{3}$ rule used to avoid aliasing errors.

Since we are interested in the most unstable mode (the one with maximum growth or minimum decay), we consider a generalization of (3.6),

$$\boldsymbol{A} \frac{\mathrm{d}\boldsymbol{G}}{\mathrm{d}t} = \boldsymbol{B}\boldsymbol{G} + \boldsymbol{C}\boldsymbol{G}, \tag{3.10}$$

where $\boldsymbol{G}$ is a matrix of solution vectors. By initializing $\boldsymbol{G}$ to the identity matrix we ensure capture of the complete set of solutions. As this is a Floquet problem, we expect the solution to have the form

$$\boldsymbol{G}(t) = \boldsymbol{P}(t) \exp(t\boldsymbol{Q}), \tag{3.11}$$

where $\boldsymbol{Q}$ is a constant matrix and $\boldsymbol{P}$ is a periodic matrix; the period, τ, is imposed by the pressure and is the same as that of $\boldsymbol{C}$, the matrix containing the convective terms. We follow the procedure of Grosch & Salwen (1968) to determine the stability characteristics. Since

$$\begin{aligned} \boldsymbol{G}(0) &= \boldsymbol{I} \\ &= \boldsymbol{P}(0) \exp(0\boldsymbol{Q}) \end{aligned} \tag{3.12}$$

we have $\boldsymbol{P}(0) = \boldsymbol{I}$.

At the end of a period,

$$\begin{aligned} \boldsymbol{G}(\tau) &= \boldsymbol{P}(\tau) \exp(\tau\boldsymbol{Q}) \\ &= \boldsymbol{P}(0) \exp(\tau\boldsymbol{Q}) \\ &= \exp(\tau\boldsymbol{Q}). \end{aligned} \tag{3.13}$$

If the eigenvalues of $\boldsymbol{G}(\tau)$ are λ_j, the associated growth rates are

$$\sigma_j = \ln(\lambda_j)/\tau. \tag{3.14}$$

S	A	von Kerczek	Linear	Full
$\omega_1/22$	0.20	$+5.0\times10^{-3}$	$+5.6\times10^{-3}$	$+4.8\times10^{-3}$
$\omega_1/7$	0.20	-8.0×10^{-3}	-7.7×10^{-3}	-8.2×10^{-3}
$\omega_1/3$	0.05	-2.2×10^{-3}	-2.2×10^{-3}	-2.2×10^{-3}
$\omega_1/3$	0.20	-2.6×10^{-2}	-2.7×10^{-2}	-2.7×10^{-2}
ω_1	0.10	-1.0×10^{-3}	-1.0×10^{-3}	-1.1×10^{-3}
ω_1	0.25	-5.5×10^{-3}	-5.3×10^{-3}	-5.3×10^{-3}
$2\omega_1$	0.20	-4.1×10^{-4}	-5.7×10^{-4}	-5.7×10^{-4}
$4\omega_1$	0.20	-5.1×10^{-5}	-4.3×10^{-5}	-5.2×10^{-5}
$16\omega_1$	0.20	$+4.6\times10^{-9}$	$+4.6\times10^{-5}$	-3.9×10^{-6}

TABLE 1. Comparison of growth rates: $Re = 5772.22$, $k_x = 1.0206$, $\omega_1 = 0.2694$

A positive real part of σ_j indicates growth, a negative value indicates decay. Experience with the steady Orr–Sommerfeld equation suggests that the least-stable mode has a real part small relative to its imaginary part. To avoid polluting the small growth rate, we use a time-advance scheme which is reversible; integration of (3.10) is performed with the Crank–Nicolson method.

To compare our results with those of von Kerczek, we tested the code at $Re = 5772.22$ and non-dimensional two-dimensional wavenumber $k_x = 1.0206$. For this case, the Tollmien–Schlichting (TS) wave with non-dimensional frequency $\omega_1 = 0.2694$ is neutrally stable for steady flow and the critical layers are $0.14h$ from the walls. The growth rates calculated by von Kerczek, our linear code, and our full numerical simulation are given in Table 1. Von Kerczek's results for $S < \omega_1$ were estimated from his figure 1; growth rates for $S \geqslant \omega_1$ were calculated from his table 3. Von Kerczek estimates his results to be accurate to at least one significant digit. In our linear code 50 polynomials were used for $\omega < 2\omega_1$ which guarantees a minimum of seven grid points in each Stokes layer. Using 75 polynomials changed the growth rates by less than 0.1 %. At higher frequencies, the Stokes layer was not well resolved. However, at high frequencies the effects of the oscillation are small and our approach is not well suited to accurate calculation of the minute growth rates. Considering these difficulties, the results of our linear code are in good agreement with those obtained by von Kerczek. Since the method used in our work is essentially that of Grosch & Salwen (1968), we suspect that their erroneous results were due to lack of resolution of the Stokes layers.

3.2. *Results*

Including the unsteady mean flow in the full simulation code described in Singer, Ferziger & Reed (1987*a*) provides the results given in the last column of Table 1. Up to Strouhal number $S = 2\omega_1$ the growth rates calculated from the full simulation agree well with those of our linear code and von Kerczek. At higher Strouhal numbers, the Stokes layer in our work is not sufficiently resolved.

To compare with our earlier computations (Singer, Reed & Ferziger 1986, 1987*b*), we used a Reynolds number of 5000. For steady mean flow, this Reynolds number is in the linearly stable regime. Fifty polynomials were used. The thickness of the Stokes layer at the highest frequency, $S = 3.155$ was $\delta = 0.0112$ and contained five grid points. Calculations with 75 polynomials gave results that differed by less than 1.5 % at all Strouhal numbers.

Figure 2(*a*) gives the growth rates as a function of oscillation amplitude and frequency at $Re = 5000$; they are similar to von Kerczek's results at $Re = 5772.22$.

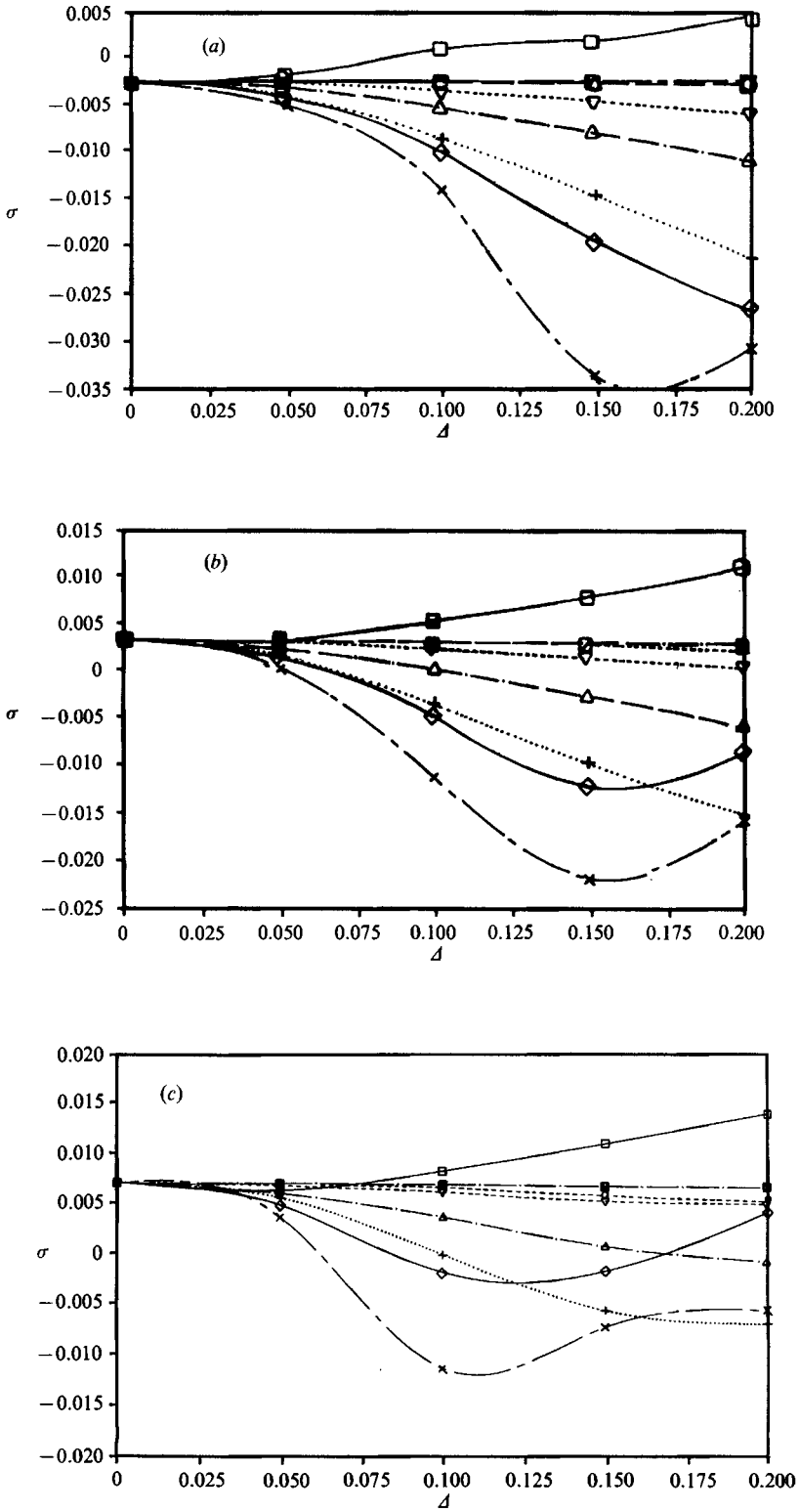

FIGURE 2 (*a–c*). For caption see facing page.

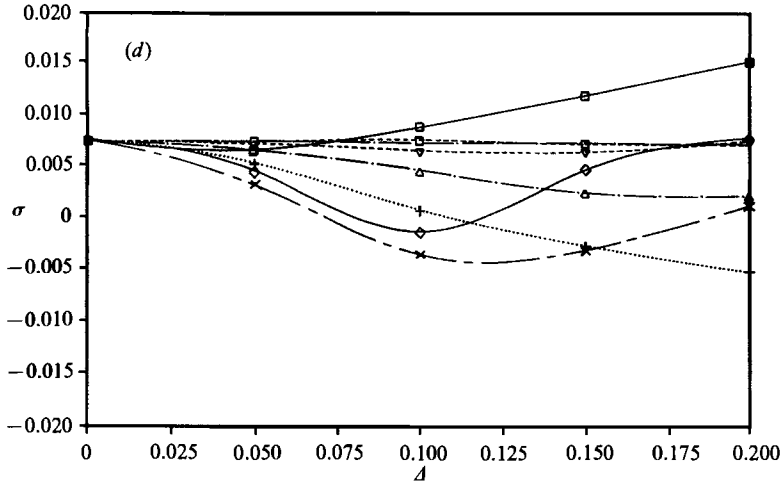

FIGURE 2. Oscillating mean flow linear growth rates (σ) versus maximum fractional change in velocity (Δ). (*a*) $Re = 5000$, $k_x = 1.12$, $\omega_1 = 0.3155$. (*b*) $Re = 10000$, $k_x = 1.0$, $\omega_2 = 0.2375$. (*c*) $Re = 25000$, $k_x = 0.84$, $\omega_1 = 0.1561$. (*d*) $Re = 47000$, $k_x = 0.78$, $\omega_1 = 0.1247$. □, $\eta = 1.31$; ○, $\eta = 0.74$; Δ, $\eta = 0.62$; +, $\eta = 0.52$; ×, $\eta = 0.40$; ◇, $\eta = 0.33$; ▽, $\eta = 0.23$; ⊠, $\eta = 0.17$; ✳, $\eta = 0.10$; ⊕, $\eta = 0.074$.

Figure 2(*b*) showed the results at $Re = 10000$. In these figures, the frequency parameter is the ratio of the Stokes layer thickness to the critical layer height of the steady-flow TS wave. The non-dimensional distance from the wall to the critical layer is

$$d_c = 1 - |y_c|, \tag{3.15}$$

where y_c is the height at which the phase speed of the TS wave is equal to the speed of the mean flow in the steady case. Thus the frequency parameter is

$$\eta = \delta / d_c. \tag{3.16}$$

Increasing the frequency decreases η. For the same value of η, the curves have approximately the same shapes. The behaviour with increased oscillation strength is not monotonic at the most stabilizing frequencies. Except at the lowest frequency ($\eta = 1.31$), the oscillations stabilize the flow. Provided that the streamwise wavenumber is approximately that of the least stable wave, the most stabilizing frequency for Reynolds numbers up to 47000 corresponds to $\eta \approx 0.40$; η increases slightly with increasing Reynolds number. At higher Reynolds numbers, Squire's theorem shows that certain three-dimensional waves grow with the maximum amplification rate realized by a two-dimensional wave at the lower Reynolds number (Magen & Patera 1986).

Our results at $Re = 25000$ and $Re = 47000$ (figures 2*c* and *d*) indicate that the linear growth rate curves depend only weakly on the Reynolds number. Increasing the Reynolds number decreases the effects of oscillation.

Another normalization of the frequency can be obtained with the ratio of a lengthscale based on $(\nu/\omega_1^*)^{\frac{1}{2}}$ (where an asterisk indicates a dimensional quantity) and the Stokes layer thickness. This is proportional to $(\Omega^*/\omega_1^*)^{\frac{1}{2}}$, and was used by Grosch & Salwen (1968), while the square of this quantity was used by von Kerczek (1982) and Singer *et al.* 1987*a*). Our data indicate that both normalizations work well.

The nonlinear behaviour of this flow is closely connected with its linear behaviour.

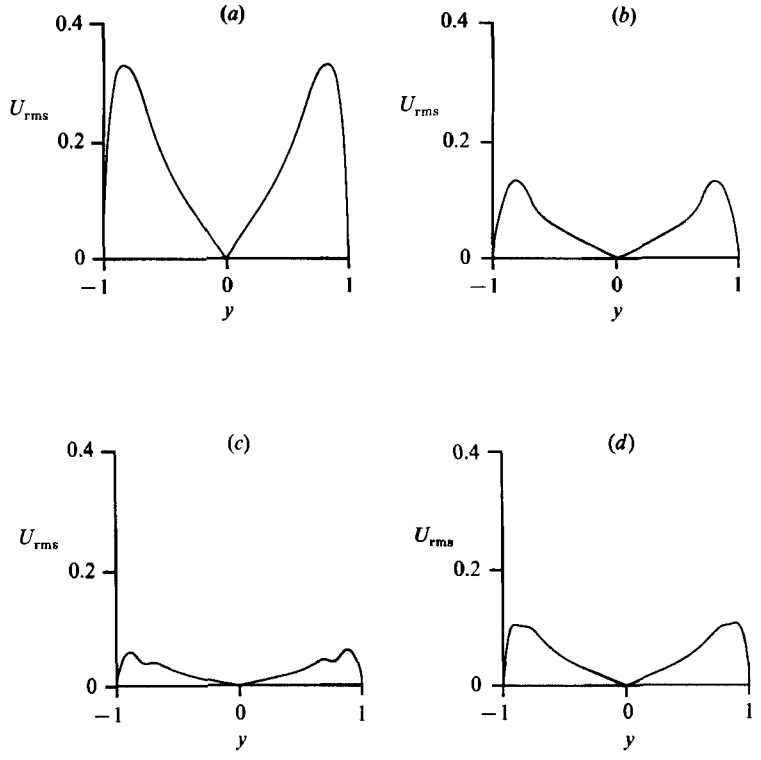

FIGURE 3. Computed r.m.s. streamwise velocity of a two-dimensional wave based on the linearized equation with $k_x = 1.12$, $Re = 5000$, $S = 0.1051667$ ($\eta = 0.40$), and $\Delta = 0.10$ at (*a*) $t = 14.93$, (*b*) 29.87, (*c*) 44.81 and (*d*) 59.74.

The average growth or decay of a wave over a cycle was given above. It is also important to consider the detailed behaviour. As a typical case, consider $S = 0.1051667$ ($\eta = 0.40$), $\Delta = 0.10$; the mean flow was described above. Since the mean flow is symmetric about the centreline, references to mean flow features will be restricted to one side of the channel.

To study the linear evolution of a two-dimensional wave, we solve (3.6) with an initial condition vector whose elements are all unity. After just one cycle, the profile becomes periodic and therefore independent of the initial conditions. Results are given for the second period but, for comparison with our previous results, we report the times as if it were the first cycle. Instantaneous growth rates are computed from

$$\sigma(t) = \frac{\mathrm{d} \ln |g(t)|}{\mathrm{d}t} = \frac{1}{|g(t)|} \frac{\mathrm{d}|g(t)|}{\mathrm{d}t}, \tag{3.17}$$

where $|g(t)|$ is the L_2-norm of $g(t)$. 300 time steps per cycle were used; using 200 time steps per period gave results that were indistinguishable from these. First-order backward differences are used to calculate time derivatives; this is sufficiently accurate. As a test, we ran a case with $\Delta = 0$; the instantaneous growth rate was within 0.2 % of the growth rate of the least stable steady-flow eigenmode. The dotted line in figure 6(*b*) shows the instantaneous linear growth rate versus time. The maximum positive growth rate occurs when the extent of positive curvature near each wall is large. Figure 3(*a*) gives the r.m.s. streamwise perturbation velocity distribution at $t = 14.93$. There are no inflection points in the flow at this time; the

instantaneous growth rate (cf. figure 6*b*) is negative and the profile resembles a TS wave. At $t = 29.87$, the r.m.s. streamwise velocity distribution is shown in figure 3(*b*) and as figure 6(*b*) indicates, the decay is very strong. Next comes the most unusual phase of the cycle; at $t = 44.81$, the streamwise velocity distribution has a double peak structure (cf. figure 3*c*). A second inflection point has just appeared in the flow, there is a large region of positive curvature, and the disturbance has a large positive growth rate. The double peak structure is associated with the fact that the mean flow is drawing energy from the two-dimensional wave in the region between the peaks. This will be discussed in a later section. At the end of the period, $t = 59.74$, there is still positive growth and figure 3(*d*) shows that the structure is again similar to a TS wave.

As the frequency of oscillation goes to zero, (2.2) and (2.3) indicate that the mean flow can be approximated by a parabolic profile with a slowly varying amplitude if the quantity $\frac{1}{2}(NReS) \ll 1$. This condition is never satisfied by our base flows, hence it is not surprising that computations show that a quasi-steady stability analysis poorly predicts the instantaneous growth rates for our cases. Von Kerczek (1982) came to a similar conclusion.

4. Nonlinear simulations

4.1. *Parameter description*

Since the flow seems to be relatively insensitive to the Reynolds number, all direct simulations were performed at $Re = 5000$. The code described by Singer *et al.* (1987*a*) was used. (The original version was written by Moser using the method of Moser *et al.* 1983.) This allowed comparison with steady mean flow results at the same Reynolds number (Singer *et al.* (1986, 1987*b*). The spatial resolution was 16, 32 and 64 modes in the streamwise, spanwise and normal directions respectively. This provides approximately the same resolution in the normal direction as in the linear two-dimensional simulations. The time step was chosen to allow at least 100 time steps per period of mean flow oscillation. For cases in which two-dimensional simulations indicated that the flow would change rapidly, smaller time steps were used. The maximum CFL number never exceeded one half of the limiting value allowed by the numerical method.

Only two initial phases of the mean flow oscillation were used; the initial pressure gradient was either maximum or minimum. In the following, a positive value of Δ indicates a favourable initial pressure gradient ($\mathrm{d}p/\mathrm{d}x < 0$); a negative value of Δ indicates an adverse initial pressure gradient ($\mathrm{d}p/\mathrm{d}x > 0$). Starting the computation with an adverse pressure gradient produces nonlinear effects that are not observed if the initial noise is first 'cleaned up' with a favourable pressure gradient.

Simulations were performed with four magnitudes of the maximum fractional velocity change; $|\Delta| = 0.10$, 0.12, 0.15 and 0.20. The linear growth rates indicated that the effects of the oscillations are strongest for $|\Delta| > 0.10$. Stronger mean flow oscillations probably cannot be obtained in even carefully controlled wind tunnels without the addition of higher harmonics; therefore Δ was limited to 0.020.

At least one simulation was performed at each of the following Strouhal numbers: $S = 0.01$, 0.031 55, 0.105 17, and 1.262. If the frequencies are expressed in terms of the ratio of the Stokes layer thickness to the steady-flow critical layer height, these correspond to: $\eta = 1.31$, 0.74, 0.4, 0.12 and include (1) a very low, linearly destabilizing frequency, (2) a low, slightly stabilizing frequency, (3) a moderate, strongly stabilizing frequency, and (4) a high frequency.

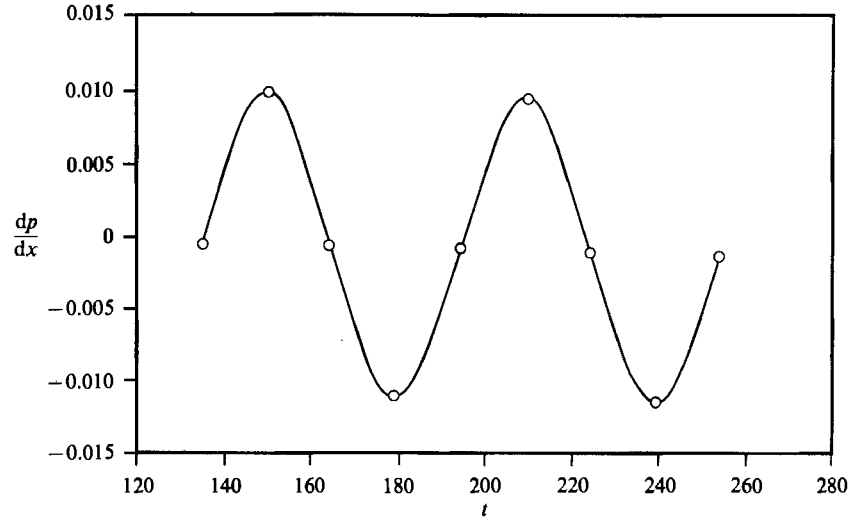

FIGURE 4. Mean-flow pressure gradient versus time. $\eta = 0.40$, $\Delta = 0.10$.

Initial TS waves with a variety of initial amplitudes were used in our runs. Many of the cases were performed without a TS wave; in these cases, the structures grow out of the initially random background noise.

In unsteady simulations, the initial amplitude of the random noise, ϵ, may be important. At the start of a simulation, random numbers between $-\epsilon$ and ϵ are added to each Fourier component of the velocity at each y. We performed simulations with $\epsilon = 10^{-5}$ and 10^{-4}. Increasing ϵ is always destabilizing.

4.2. *Results*

We expect the nonlinear behaviour to be correlated with the linear behaviour. At $Re = 5000$, the latter is principally determined by the frequency parameter η. From figure 2(*a*), we can discriminate four frequency ranges. At high frequency, differences from the steady case are minor. At intermediate frequencies there is strong stabilization. At lower intermediate frequencies there is little effect on the *linear* growth rates but nonlinear effects are important. Finally, low-frequency oscillations are linearly destabilizing. We conjecture, on the basis of figure 2(*a–d*) that these results hold at other Reynolds numbers, at least with $\Delta < 0.15$. While both high-frequency and moderate-to-low-frequency oscillations have little effect on the *linear* stability of the flow, we show below that the nonlinear behaviour may be quite different.

4.2.1. *High frequency* ($0.2 > \eta$)

The least interesting case is one in which the forcing frequency is more than twice the TS frequency. In this case, the perturbations act as if there were no oscillation, even with mean-flow velocity variations of 20% of the steady-flow centreline velocity, U_0. At this Strouhal number, the Stokes layers near the walls are very thin and do not interact with the TS waves. Most of the flow maintains the parabolic profile, the instantaneous Reynolds number simply oscillates. The oscillation is rapid and the disturbances behave much as they would at the average Reynolds number.

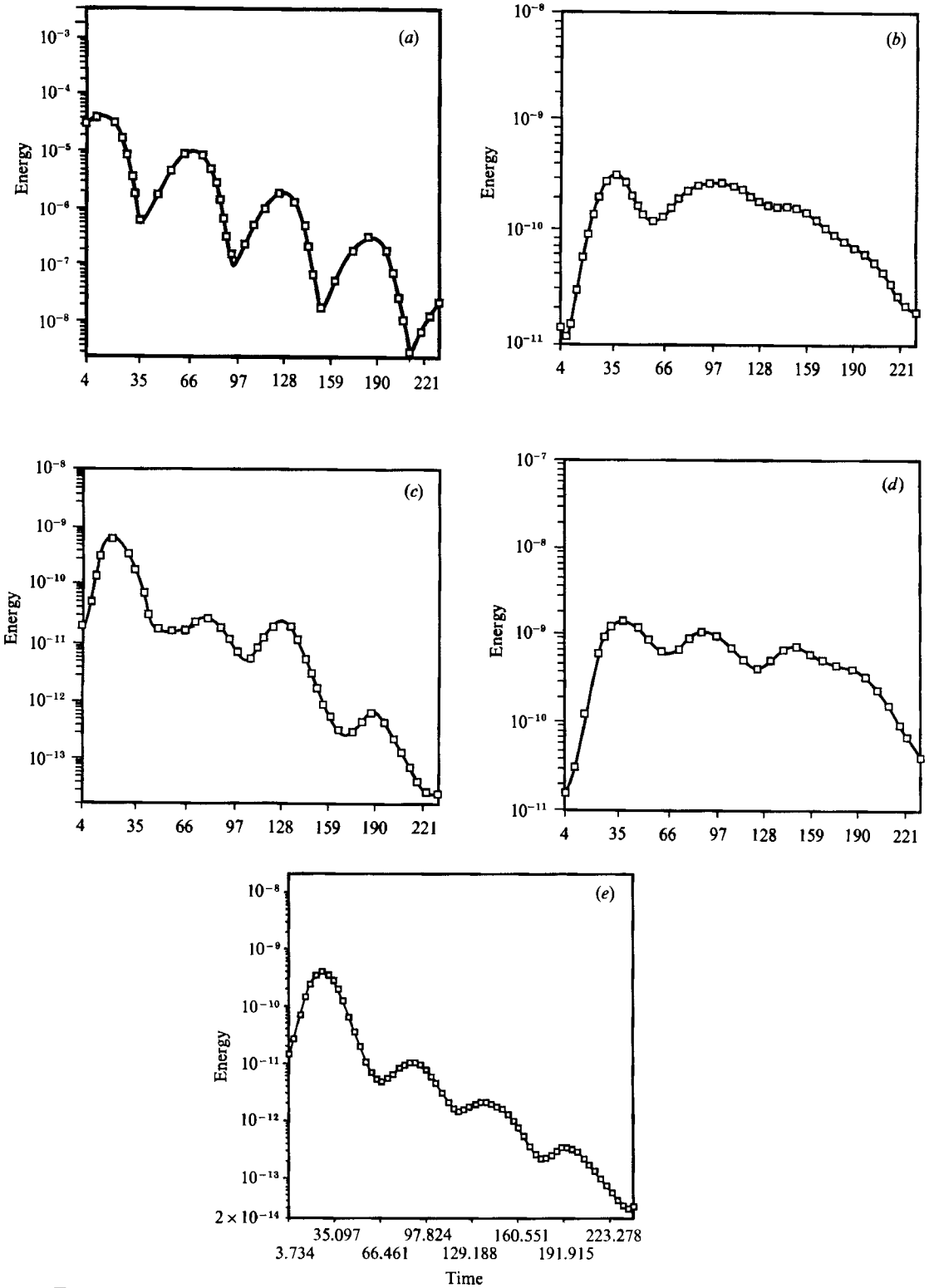

FIGURE 5. Evolution of the energy in various waves. $\eta = 0.40$, $\Delta = 0.10$. (*a*) $k_x = 1.12$, $k_z = 0$, (*b*) $k_x = 0.56$, $k_z = 0.9$, (*c*) $k_x = 1.12$, $k_z = 0.9$, (*d*) $k_x = 0.56$, $k_z = 1.8$, (*e*) $k_x = 1.12$, $k_z = 1.8$.

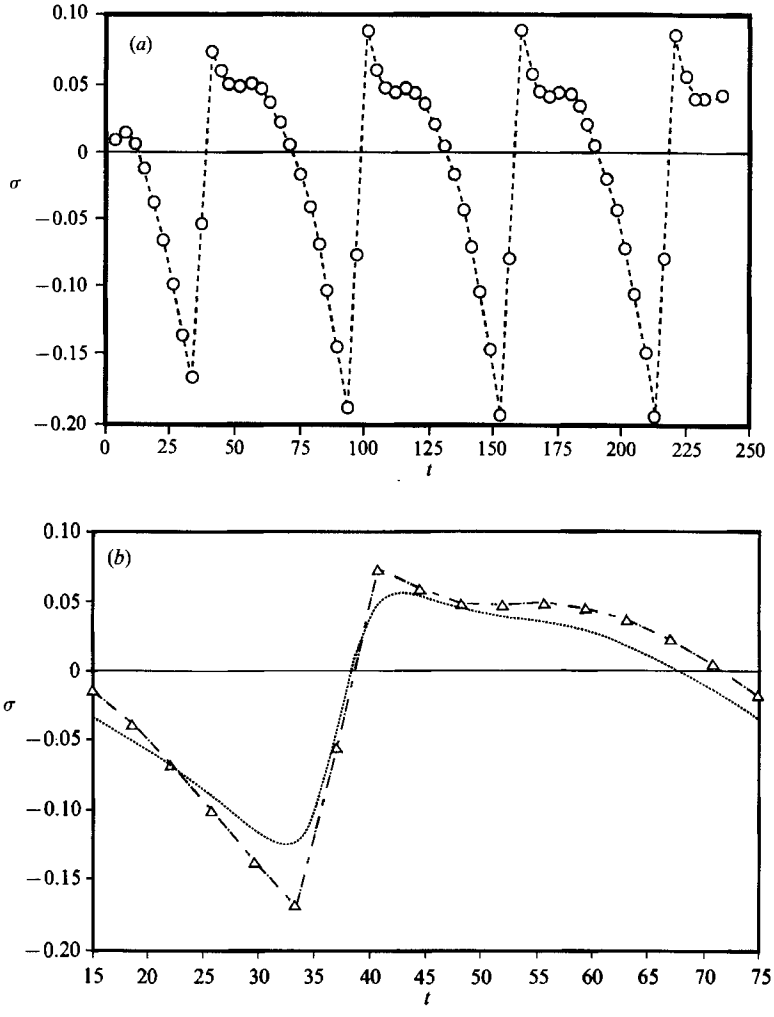

FIGURE 6. Instantaneous growth rates with $k_x = 1.12$, $Re = 5000$, $S = 0.1051667$ ($\eta = 0.40$), and $\Delta = 0.10$. (*a*) Full simulation, (*b*) ·····, two-dimensional, linear simulation; ——, three-dimensional nonlinear simulation with region $75 < t < 135$ enlarged and rescaled.

4.2.2. *Moderate frequency* ($0.6 > \eta > 0.2$)

In this range the TS wave is strongly damped in the presence of mean-flow oscillation. Consider a case with $\eta = 0.40$, $\Delta = 0.10$, and an initial TS wave with r.m.s. streamwise velocity of 2% of U_0. Without oscillation, this flow would be unstable; with oscillation it is stable. At this (and greater) frequencies, the two-dimensional wave reaches its asymptotic state during the initial period. Velocity fields were examined at each phase for which mean-flow and linear results were presented. For reference, figure 4 provides the pressure gradient as a function of time. Symbols correspond to the velocity field considered.

Figure 5(*a*) shows the time evolution of the energy in the two-dimensional TS wave. The variation is damped-periodic but the decreases in energy are steeper and more severe than the rises. Figure 6(*a*) shows the instantaneous growth rate of this wave; it was computed at the times indicated by the circles using a time step of 1/400

of the oscillation period. Local energy maxima occur when the growth rate becomes negative; local minima appear at phases at which the growth rate becomes positive. To compare the growth rates with those obtained from linear theory, we enlarge the region from $t = 75$ to $t = 135$ and subtract the equivalent of one period from the abscissa. Both linear and nonlinear simulation instantaneous growth rates are shown in figure 6(*b*). The agreement away from the region of strong gradients in the growth rates is satisfactory; the differences are probably due to the mean-flow distortion in the direct numerical simulation.

The energy histories of three-dimensional waves, illustrated in figures 5(*b–e*), indicate that qualitative application of Herbert's (1983) secondary instability theory to the unsteady flow is useful. The two three-dimensional subharmonics shown in figures 5(*b*) and 5(*d*) experience very little net decay during the first two cycles of the mean flow. After the third peak in the primary two-dimensional wave at $t = 131$, the r.m.s. amplitude of the streamwise component of the two-dimensional wave has been reduced to 0.44% of U_0 and the three-dimensional waves experience much more rapid decay. This amplitude of the two-dimensional wave is near the critical level required to support the subharmonic secondary instability in steady flow. The critical amplitude needed to support fundamental (K-type) modes in steady flow is greater than that required to support the H-type modes. In consequence, the two three-dimensional fundamental modes shown in figures 5(*c*) and 5(*e*) decay after the first period. This leads us to believe that the mechanisms in oscillating flow are similar to those in steady flow. However, quantitative extension of Herbert's theory to unsteady mean flows would be very difficult. Structural varations of the two-dimensional wave are major difficulties. Also, the growth/decay of the primary two-dimensional wave increases the importance of the strength of the background noise in determining not only when, but whether, transition will occur. Similarly, the initial phase of the flow can be important; an initially decaying two-dimensional wave requires a larger initial amplitude or a higher level of random noise to induce transition than an initially growing wave. Finally, the instantaneous growth rates of the two-dimensional wave are comparable with those of the three-dimensional secondary waves, invalidating the quasi-steady assumption in Herbert's theory. It is unlikely that a quasi-steady secondary instability analysis would give results in accord with direct numerical computations.

We now look at the r.m.s. streamwise velocity distributions of three selected waves. In particular, we compare the evolution of the two-dimensional wave with the prediction of linear theory, and the evolution of the dominant three-dimensional waves with those in previous simulations.

Figure 7(*a–d*) shows profiles of the two-dimensional wave through one cycle. The sequence of figures starts at $t = 134$, slightly after a peak in the energy. The two-dimensional profiles are almost identical to those of the linear two-dimensional simulation shown in Figure 3(*a–d*); the behaviour of the primary two-dimensional wave is essentially linear. To obtain further insight into the unusual deformation of the two-dimensional wave in figure 7(*c*) we shall use the energy-transfer-rate analysis developed in Singer *et al.* (1987*c*).

Figure 8 shows the energy transfer rate from the primary two-dimensional wave to the mean flow integrated over horizontal planes as a function of normal coordinate at the time corresponding to figure 7(*c*). At this phase, there are two peaks in the profile of $u_{\text{r.m.s.}}$. There is a great deal of energy transfer to the two-dimensional wave near the centreward peaks and a considerable energy transfer *away* from the two-dimensional wave in the region between the twin peaks. This indicates that

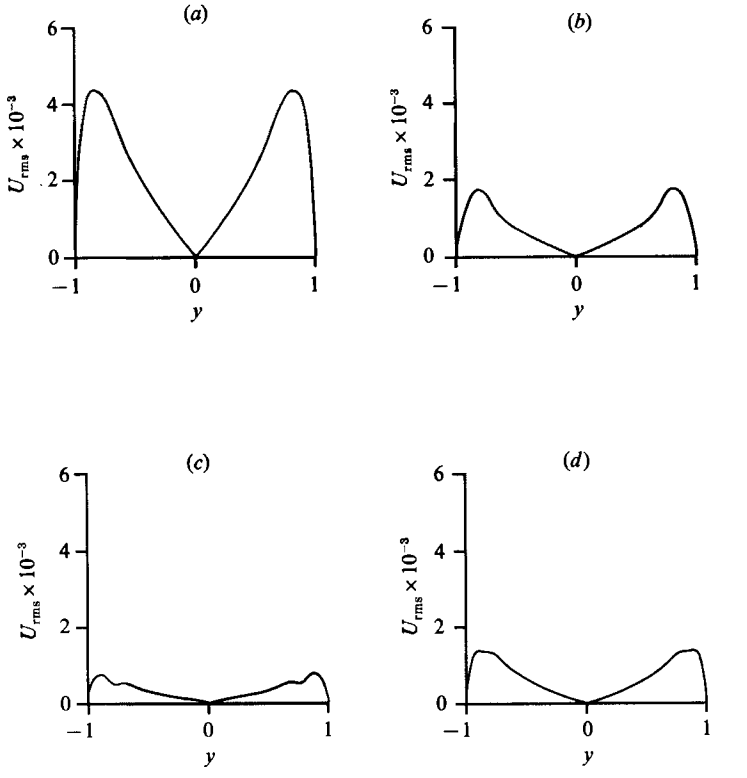

FIGURE 7. Profiles of r.m.s. streamwise velocity of the two-dimensional wave ($k_x = 1.12$, $k_z = 0$) for $\eta = 0.40$, $\Delta = 0.10$. (*a*) $t = 134.4$, (*b*) 149.4, (*c*) 164.3, (*d*) 179.2.

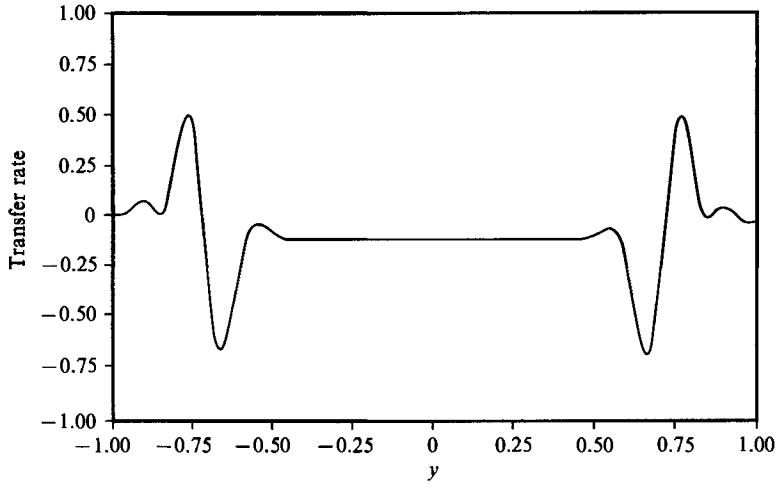

FIGURE 8. Energy-transfer rates to the mean flow from the primary two-dimensional wave in oscillating pressure gradient flow, $\eta = 0.40$, $\Delta = 0.10$ and $t = 164.3$.

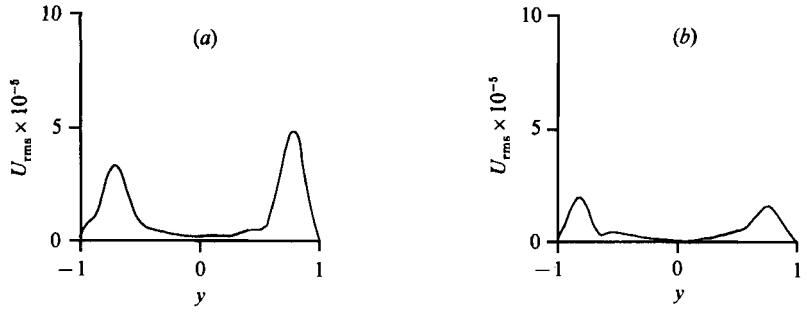

FIGURE 9. Profiles of r.m.s. streamwise velocity of the subharmonic three-dimensional wave ($k_x = 0.56$, $k_z = 0.9$) for $\eta = 0.40$, $A = 0.10$. (*a*) $t = 179.2$, (*b*) 239.0.

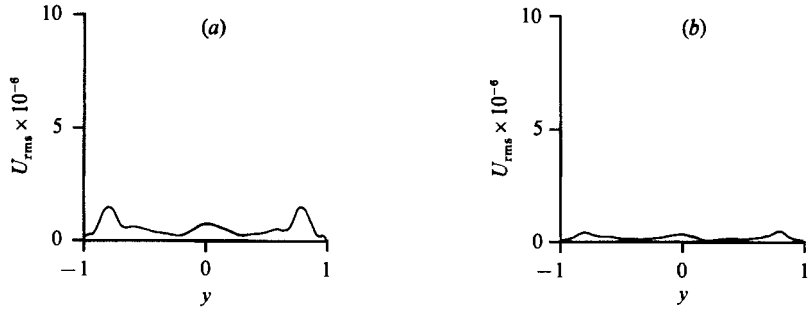

FIGURE 10. Profiles of r.m.s. streamwise velocity of a fundamental three-dimensional wave ($k_x = 1.12$, $k_z = 0.9$) for $\eta = 0.40$, $A = 0.10$. (*a*) $t = 179.2$, (*b*) 239.0.

interaction between the unsteady mean flow and the disturbance is responsible for this deformation.

Figures 9(*a*) and 9(*b*) show the distribution of the r.m.s. streamwise velocity of the subharmonic wave ($k_x = 0.56$, $k_z = 0.9$) at the end of two consecutive periods. The profiles are not periodic. Two factors contribute to the aperiodicity of these structures. Subharmonic modes are asymmetric; the energy tends to concentrate on one side of the channel and then slowly shift to the other side. The behaviour of this wave is also strongly dependent on the amplitude of the two-dimensional wave. While the profile of the two-dimensional wave is periodic, in part of the cycle, its amplitude decreases to a point insufficient to support the subharmonic instability.

Growth of fundamental (K-type) modes requires a higher amplitude primary two-dimensional wave. Since the subharmonic mode is stable, the fundamental mode should also be stable. Figure 10(*a*, *b*) shows the amplitude distribution of a fundamental mode ($k_x = 1.12$, $k_z = 0.9$). There is a local maximum near the channel centre; this is most apparent in the last cycle, figure 10(*b*). The central bulge is not characteristic of K-type modes. 'Centre modes' in which u is symmetric are the linearly least stable three-dimensional structures at this wavevector for steady flow without a two-dimensional wave. Thus, the structure is a combination of a K-type mode, which decays more and more rapidly as the primary two-dimensional wave dwindles, and the 'centre mode' that is left behind.

To demonstrate that the above mean flow can undergo transition, we performed a simulation with a two-dimensional wave of $A = 5\%$. The flow undergoes transition via secondary instability. Figure 11 shows the energy in the most energetic

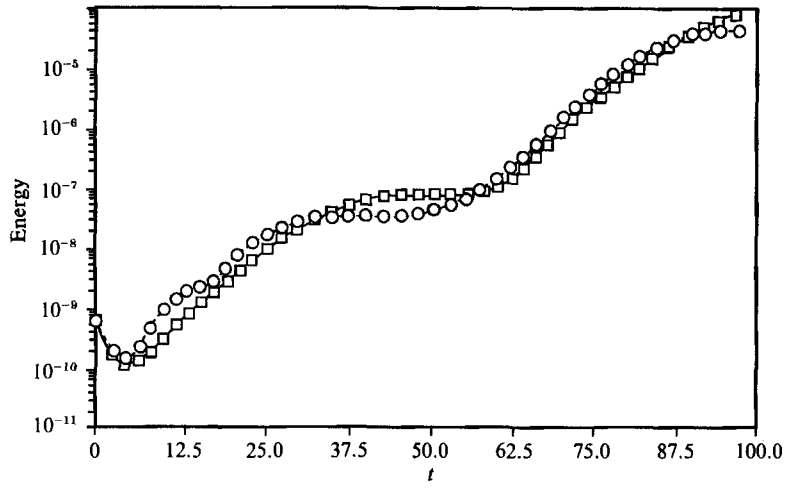

FIGURE 11. Energy history of most energetic □, subharmonic ($k_x = 0.56$, $k_z = 1.8$) and ○, fundamental ($k_x = 1.12$, $k_z = 2.7$). $\eta = 0.40$, $\Delta = 0.10$, $A = 5\%$.

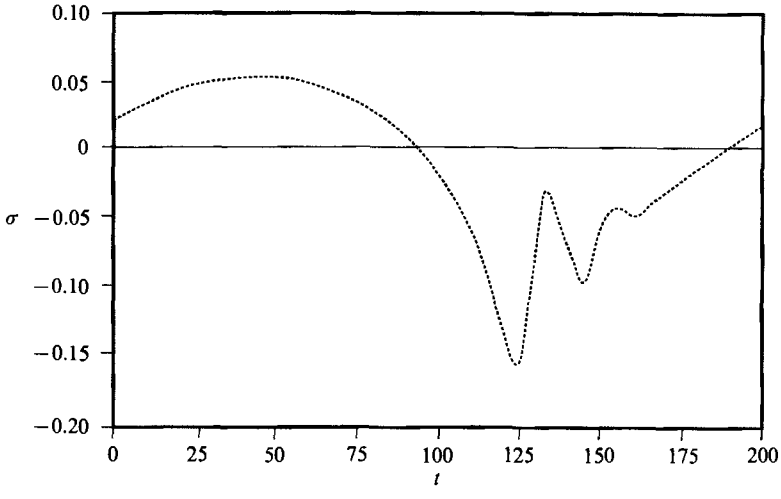

FIGURE 12. Instantaneous two-dimensional linear growth rates with $k_x = 1.12$, $Re = 5000$, $\eta = 0.74$ ($S = 0.031\,55$), and $\Delta = -0.12$.

subharmonic and fundamental modes. The two are competitive at this two-dimensional amplitude. The smaller scales develop slightly more slowly than for a similar case without mean-flow oscillation. The resolution was insufficient to reliably simulate events after the development of small scales. We saw no indication of relaminarization after the small scales developed, even during linearly stabilizing phases.

4.2.3. *Moderately low frequency* ($1 > \eta > 0.6$)

As illustrated in figure 2(*a*), in this frequency range the mean-flow oscillation has little effect on the linear growth rates. This range lies between the destabilizing low-frequency modulations and the highly damped moderate frequency modulations. In this range, the primary two-dimensional wave experiences energy variations of

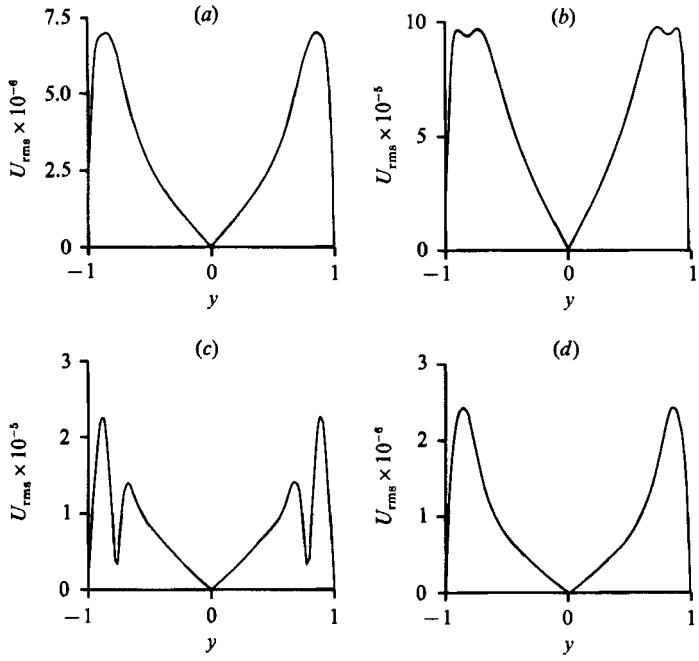

FIGURE 13. Profiles of r.m.s. streamwise velocity of the two-dimensional wave ($k_x = 1.12$, $k_z = 0$) for $\eta = 0.74$, $\Delta = -0.12$. (*a*) $t = 199$, (*b*) 249, (*c*) 315, (*d*) 382. Note the large changes in the scale of the ordinate.

approximately 10^5 when $\Delta = -0.12$. Owing to the large variations of the energy in the two-dimensional wave at this frequency, it was not necessary to include one in the initial conditions; the two-dimensional wave evolves from the initial random noise, as in a 'natural' transition.

For the case in which $\eta = 0.74$, $\Delta = -0.12$, figure 12 illustrates the instantaneous two-dimensional linear growth rates for the second cycle. Although the instantaneous growth rates are more jagged than for $\eta = 0.40$, the maximum growth rates still occur during phases in which there is a large region of positive curvature of the mean velocity profile. Figure 13(*a–d*) shows the r.m.s. streamwise velocity perturbations of this wave at four phases during the second cycle of oscillations. A double-peaked structure (cf. figure 13*b*) appears during phases of large growth; it is stronger at the phase in which there are no inflection points and the two-dimensional wave decays (cf. figure 13*c*). The instantaneous growth rates fluctuate rapidly near this phase, probably owing to interference between the disturbances and the mean flow.

Similar fluctuations in the instantaneous growth rates were reported by von Kerczek (1982) for a case with $Re = 5772.22$, $\eta = 0.94$, and $\Delta = 0.25$. He finds a long stretch of positive growth when there is possible curvature in the mean velocity profile (cf. his figure 4). He suggests that there is competition between quasi-steady eigenmodes. However, unless the average growth rates of different eigenmodes are approximately equal, the amplitudes of the various modes will change relative to each other during each cycle. Then the fluctuations in the instantaneous growth rates will differ from cycle to cycle since the amplitudes of the competing eigenmodes would also differ. Our data indicate that the instantaneous growth rates become periodic by the conclusion of the first cycle indicating that intermodal competition probably does not play a major role in this flow.

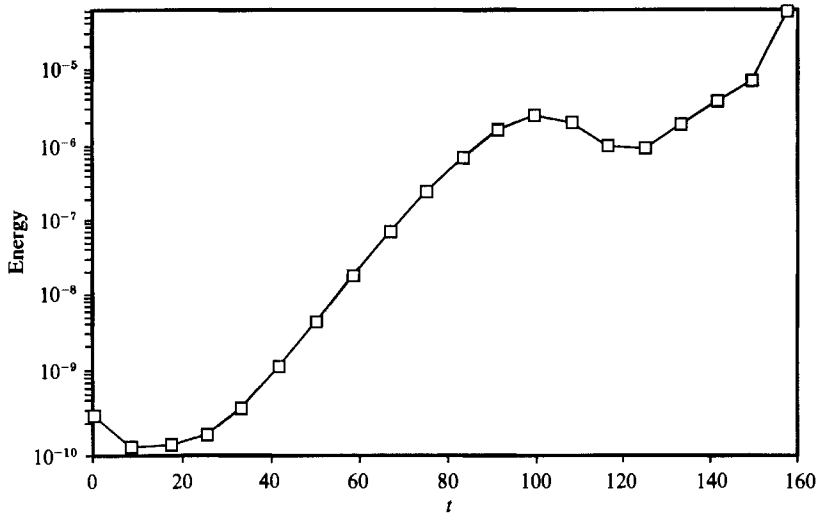

FIGURE 14. Energy history of the two-dimensional wave ($k_x = 1.12$, $k_z = 0$) for $\eta = 0.74$, $\Delta = -0.20$.

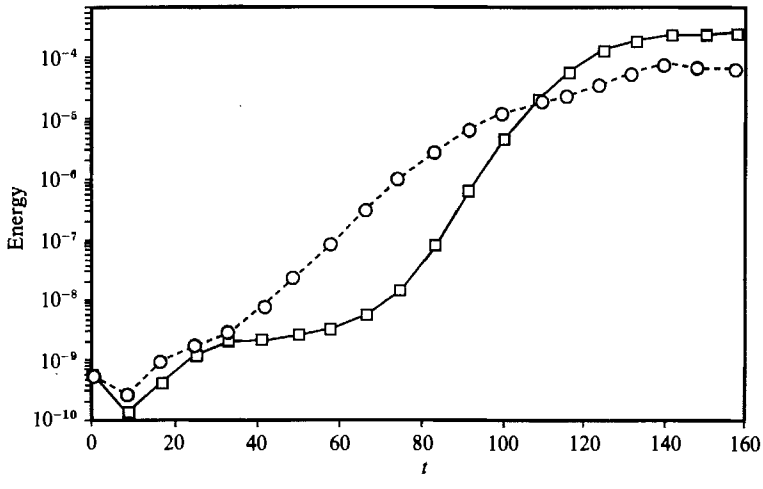

FIGURE 15. Energy history of most energetic □, subharmonic ($k_x = 0.56$, $k_z = 0.9$) and ○, fundamental ($k_x = 1.12$, $k_z = 0.9$). $\eta = 0.74$, $\Delta = -0.20$.

The large variations in the energy of the two-dimensional wave at this frequency were able to trigger transition without the inclusion of a primary two-dimensional wave in the initial conditions. With $\eta = 0.74$ and $\Delta = -0.20$, the two-dimensional wave grew so rapidly that a secondary instability led to transition during the first cycle. Figure 14 illustrates the energy evolution of the two-dimensional wave. The energy histories of the most energetic subharmonic and fundamental modes are illustrated in figure 15. All of the disturbances grow rapidly from an initial condition of random noise and show no indication of relaminarization. This case is interesting since the initial level of random noise was in the linear range. Even though the flow is linearly stable in the Floquet sense (cf. figure 2*a*), instantaneous strength of the two-dimensional wave can initiate nonlinear secondary instability.

5.2.4. *Low frequency* ($\eta > 1$)

At very low Strouhal numbers, the flow is linearly unstable with respect to the two-dimensional wave. The oscillations in the energy of the unstable two-dimensional wave are very large. For $\eta = 1.31$ and $\Delta = -0.12$ the energy varies by 10^6 in a single period. This means that very small two-dimensional disturbances can reach amplitudes large enough to support secondary instability during part of the cycle.

An interesting difference between the behaviour at these Strouhal numbers and that at higher Strouhal numbers lies in the evolution of the two-dimensional wave. In this case, the double-peak structure in the r.m.s. streamwise velocity profile was not observed. The instantaneous growth rates of the two-dimensional wave are much smoother than at larger Strouhal numbers, though the maxima still occur during phases in which there are large regions of positive curvature.

We performed one simulation designed to determine the importance of the two-dimensional wave by artificially setting it to zero at each time step. The computation was performed with $\eta = 1.31$, $\Delta = -0.12$, and $\epsilon = 10^{-4}$. When allowed to evolve naturally, this flow was unstable. Elimination of the two-dimensional wave stabilized the flow, indicating that the breakdown mechanism in the oscillating case is similar to the secondary instability mechanism of the steady case.

5. Conclusions

We studied the early stages of transition in oscillatory plane Poiseuille flow. Our linear results agree with those of von Kerczek but disagree with those of Grosch & Salwen. We suspect that Grosch & Salwen did not adequately resolve the Stokes layers.

With respect to scaling, we found that the oscillation frequency is well normalized by incorporating it into the ratio of the Stokes layer thickness to the steady-flow critical layer height. Mean-flow oscillations are generally stabilizing. The most stabilizing frequency has a ratio of Stokes layer thickness to distance from the wall to the steady-flow critical layer of $\eta = 0.4$. Very high-frequency oscillations have little effect; very low-frequency oscillations are slightly destabilizing.

The nonlinear evolution of the least-stable two-dimensional wave is similar to its linear behaviour. Maximum growth rates occur when there are large regions of positive curvature near each wall. Streamwise r.m.s. velocity profiles of the two-dimensional wave show double-peak structures near each wall during phases corresponding to maximum instantaneous growth and decay rates. Local energy transfer rate distributions are consistent with the distortion of the two-dimensional profile during the cycle.

The secondary instability mechanism active in steady flows appears to be the principal mechanism for the growth of three-dimensionality but the behaviour is complicated by the existence of many more parameters. A strong average two-dimensional wave (compared to the steady case) is necessary to trigger transition. The phase at which the two-dimensional wave is introduced is important. Once small scales develop the development is so fast that there is no indication of relaminarization.

At moderately low Strouhal numbers, many waves experience long intervals of growth and decay; the ratio of maximum to minimum r.m.s. energy can be as large as 10^6. Transition can occur without an artificially generated wave in spite of the fact that all initial disturbances are in the linear range and the flow is linearly stable if

integrated over a cycle. At very low Strouhal numbers, similar nonlinear transition phenomena occur.

The authors thank Dr Philippe Spalart for many useful suggestions. This work was supported by the Air Force Office of Scientific Research under contract AF-84-0083. The authors gratefully acknowledge NASA Ames Research Center for providing computing resources.

REFERENCES

ABRAMOWITZ, M. & STEGUN, I. 1972 *Handbook of Mathematical Functions*. Dover.

GOTTLIEB, D. & ORSZAG, S. A. 1981 *Numerical Analysis of Spectral Methods: Theory and Applications*. Society for Industrial and Applied Mathematics, Phil., PA.

GROSCH, C. E. & SALWEN, H. 1968 The stability of steady and time-dependent plane Poiseuille flow. *J. Fluid Mech.* **34**, 177–205.

HALL, P. 1975 The stability of Poiseuille flow modulated at high frequency, *Proc. R. Soc. Lond.* A **344**, 453–464.

HERBERT, D. M. 1972 The energy balance in modulated plane Poiseuille flow. *J. Fluid Mech.* **56**, 73–80.

HERBERT, TH. 1983 Modes of secondary instability in Plane Poiseuille Flow. *IUTAM Symposium on Turbulence and Chaotic Phenomena in Fluids*.

KERCZEK, C. H. VON 1982 The instability of oscillatory plane Poiseuille flow. *J. Fluid Mech.* **116**, 91–114.

MAGEN, M. & PATERA, A. T. 1986 Three-dimensional linear instability of parallel shear flows. *Phys. Fluids*, **29**, 364–367.

MOSER, R. D., MOIN, P. & LEONARD, A. 1983 A spectral numerical method for the Navier–Stokes equations with applications to Taylor–Couette flow. *J. Comput. Phys.* **52**, 524–544.

SINGER, B. A., FERZIGER, J. H. & REED, H. L. 1987*a* Numerical simulation studies of laminar-turbulent transition in the plane channel. *Department of Mechanical Engineering, Stanford Univ., Stanford, Calif., Rep.* TF-31.

SINGER, B., REED, H. L. & FERZIGER, J. H. 1986 Investigation of the effects of initial disturbances on plane channel transition. *AIAA Paper* 86-0433.

SINGER, B., REED, H. L. & FERZIGER, J. H. 1987*b* Effects of streamwise vortices on transition in plane-channel flow. *AIAA Paper* 87-0048.

SINGER, B. A., SPALART, P., FERZIGER, J. H. & REED, H. L. 1987*c* Local intermodal energy transfer of the secondary instability in a plane channel. *AIAA Paper* 87-1202.